J Mater Sci (2008) 43:6840–6847
DOI 10.1007/s10853-008-2992-4

X-ray diffraction study on a nanostructured 18Ni maraging steel prepared by equal-channel angular pressing

M. R. Movaghar Garabagh · S. Hossein Nedjad · M. Nili Ahmadabadi

Received: 23 February 2008 / Accepted: 4 September 2008 / Published online: 1 October 2008

Abstract Starting from a hierarchically substructured, heavily dislocated, and highly alloyed martensitic structure, an 18Ni maraging steel was deformed by four passes of equal-channel angular pressing at ambient temperature. X-ray diffraction peak profile analyses according to the modified Williamson–Hall and Warren–Averbach methods were used for determination of apparent grain size, dislocation density, and character of the prevailing dislocations, aided by supplemental transmission electron microscopy. A mean grain size of about 60 nm was determined, corresponding reasonably to the mean dislocation cell size illustrated by means of transmission electron microscopy. Furthermore, a dislocation density of 1.3×10^{16} m^{-2} along with an about 5:1 ratio of screw to edge type dislocations were identified. A dislocation arrangement parameter larger than unity was determined for the present deformed structure, representing a weak dipole character of the dislocation structure and weak screening action of the strain fields of multiple dislocations.

Introduction

Great efforts are made on the fabrication of ultrafine-grained metallic materials, possessing superior combinations of strength and ductility required for high-performance structural applications. During the last decade, fabrication of ultrafine-grained metals has been well established using severe plastic deformation techniques such as equal-channel angular pressing, torsion straining under high pressure, accumulative roll bonding, etc. [1]. The process of ultrafine grain formation during severe plastic deformation, indeed, continues the evolution of deformed structures by virtue of extended generation, motion, and rearrangement of dislocations, principally encompassing the formation and rotation of dislocation cells with gradual transformation of incidental dislocation boundaries into the high-angle grain boundaries consecutively. Therefore, severely deformed metals often consist of nanocrystalline dislocation cells colonized in the configuration of larger, elongated, and equiaxed dislocation cell blocks, in which fraction of high-angle boundaries depends on the prevailing deformation conditions and intrinsic characteristics of the studied alloys, e.g. stacking-faults energy, phase composition, etc. [2]. According to the hierarchical multiscale substructure, severely deformed metals are usually included within the nanostructured fashion in the literature [3].

An industrially overwhelming attempt for fabrication of ultrafine-grained steels was introduced by Japanese researchers several years ago, in which the evolution of the deformed structure is accelerated by deformation of a starting martensitic microstructure [4]. In plain-carbon and low-alloyed steels up to about 0.3 wt.% carbon, and in iron–nickel alloys up to about 28 wt.% nickel, the martensite phase exhibits a "lath" morphology which has been well recognized to be heavily dislocated and hierarchically substructured into packets, blocks, and laths [5, 6]. The transformation-induced dislocation density of lath martensite has been found in the order of the heavily deformed metals, with a lath thickness less than a few hundred

M. R. Movaghar Garabagh · S. Hossein Nedjad (✉)
Faculty of Materials Engineering, Sahand University of Technology, P.O. Box 51335-1996, Tabriz, Iran
e-mail: hossein@sut.ac.ir

M. Nili Ahmadabadi
School of Metallurgy and Materials Engineering, University of Tehran, P.O. Box 14395-731, Tehran, Iran

nanometers [7]. Morito et al. [8] reported an accelerated evolution of deformed lath martensite compared with the coarse-grained ferritic counterpart in an interstitial-free ultralow carbon steel. Furthermore, it has been reported that warm annealing of cold-rolled lath martensite causes ultrafine grain formation, as compared with severely deformed metals [9–11]. Starting from a solution-annealed lath martensite microstructure, Iranpour Mobarake et al. [12] reported ultrafine grain formation in an equal-channel angular pressed 18Ni (300) maraging steel, where further studies still remain necessary for better understanding of the severely deformed lath martensite. Recently, further insights to the microstructural characterization of severely deformed and nanostructured materials are made using novel concepts of X-ray diffraction peak profile analysis, enabling the determination of grain size, grain size distribution, internal stresses, density, and arrangement of dislocations, etc. [13]. Hossein Nedjad and Movaghar Garabagh [14] used the concepts of X-ray diffraction peak profile analysis for determination of grain size distribution and dislocation structure in a solution-annealed 18Ni (300) maraging steel, and this paper is aimed at a better understanding of a severely deformed 18Ni (300) steel by X-ray diffraction peak profile analysis.

Experimental procedure

Materials and experiments

Rectangular bars with dimensions of 10 × 10 × 60 (mm^3) were cut from a solution-annealed 18Ni (300) maraging steel with a chemical composition of Fe–17.95Ni–8.78 Co–5.01Mo–0.65Ti (wt.%). Equal-channel angular pressing was performed for four passes at ambient temperature using a die with an inner angle of 90° and an outer angle of 0° following the route B_c, in which the sample is rotated counterclockwise around its longitudinal axis by 90° after each pass consecutively. Transmission electron microscopy observations of electropolished thin foils were carried out using a PHILIPS CM200-FEG operating at 200 kV. X-ray diffraction peak profiles were measured on the electropolished bars in a Bruker AXS D8-ADVANCE diffractometer using Cu-K_α radiation of 40 kV and 50 mA with a step scanning rate of 0.001° sec^{-1}. Both of the transmission electron microscopy and X-ray diffraction were made on the transverse sections of the equal-channel angular pressed bars. Instrumental broadening was recognized using a coarse-grained, commercially pure iron sample, then subtracted from the experimental diffraction peak profiles of the studied alloy according to the Stokes method [15]. Analyses of the refined X-ray diffraction peak profiles were performed using the modified Williamson–Hall and Warren–Averbach methods in order to determine the grain size and dislocation structure, driving the diffraction peak broadening of the deformed steel.

The modified Williamson–Hall approach

The integral breadths (β) and full widths at half maximum (FWHM) of experimental diffraction peak profiles are determined as the widths of Gaussian and Cauchy functions fitted to the experimental diffraction data. Derivation of the structural peak breadths are performed according to the Stokes method as given by $\beta^2 = \beta_{exp}^2 - \beta_i^2$ for Gaussian function, and $\beta = \beta_{exp} - \beta_i$ for Cauchy function, where β, β_{exp}, and β_i are the structural, experimental, and instrumental integral breadths, respectively. Instrumental broadening is removed from the values of FWHM similarly. After the removal of the instrumental broadening from the measured breadths, the structural integral breadths or the full widths at half maximum of diffraction peak profiles are plotted versus $K^2\overline{C}$ as given by [16]:

$$\beta = \frac{1}{d} + \frac{\pi(M \cdot b)^2}{2}\rho^{1/2}(K^2\overline{C}) + O\left(K^2\overline{C}\right)^2 \quad (1)$$

$$\mathrm{FWHM} = \frac{0.9}{D} + \frac{\pi(M' \cdot b)^2}{2}\rho^{1/2}(K^2\overline{C}) + O\left(K^2\overline{C}\right)^2 \quad (2)$$

wherein d and D are the apparent size parameters. The second and third terms are related to lattice distortions raised by dislocations in which, M and M' are constants depending on the outer cut-off radius of dislocations, and O stands for higher order terms of $K^2\overline{C}$. K is the diffraction vector ($K = 2\sin\theta/\lambda$, θ is the Bragg angle, and λ is the X-ray wavelength); ρ is the dislocation density, $\overline{C}$ is the average contrast factor of dislocations, and b is the length of the Burgers vector of dislocations. Accordingly, extrapolations of β and FWHM at $K^2\overline{C} = 0$ give the apparent grain size d and D, respectively.

On the other hand, in a polycrystalline cubic metal of random orientation and random population of Burgers vectors in active slip systems, the value of $\overline{C}$ is determined by [17]:

$$\overline{C}_{hkl} = \overline{C}_{h00}\left(1 - qH^2\right) \quad (3)$$

where $\overline{C}_{h00}$ is the average contrast factor of dislocations for an (h00) reflection and q is a dislocation parameter recognizing relative fractions of screw and edge type dislocations. For a given (hkl) reflection, H^2 is given by:

$$H^2 = \frac{(h^2k^2 + h^2l^2 + k^2l^2)}{(h^2 + k^2 + l^2)^2} \quad (4)$$

Theoretical values of $\overline{C}_{h00}$ and q are determined numerically for pure screw and pure edge dislocations according to the elastic constants of the crystal.

Furthermore, turning to a squaring form of Eq. 2 and neglecting the terms of higher orders, it can be represented that [18]:

$$(\mathrm{FWHM})^2 \cong \left(\frac{0.9}{D}\right)^2 + \mu(K^2\overline{C}) \tag{5}$$

where $\mu = 2 \times \frac{0.9}{D} \times \frac{\pi(M'\cdot b)^2}{2}\rho^{\frac{1}{2}}$. By inserting Eq. 3 into Eq. 5, it can be rewritten:

$$\frac{(\mathrm{FWHM})^2 - \left(\frac{0.9}{D}\right)^2}{K^2} \cong \mu\overline{C}_{h00}\left(1 - qH^2\right) \tag{6}$$

Plotting the left-hand side of Eq. 6 vs. H^2, a linear regression is constructed using an appropriate value of $\left(\frac{0.9}{D}\right)^2$. Consequently, an experimental value of q is obtained from the intercept of the fitted line with horizontal axis to be compared with the aforementioned theoretical values of q in order to determine character of the prevailing dislocations.

The modified Warren–Averbach approach

From the Gaussian and Cauchy functions fitted to the experimental diffraction data, a Fourier transform and, accordingly, a real part of the Fourier transform are derived for experimental diffraction peak profiles. Instrumental broadening is removed according to stokes method as given by:

$$A_{\mathrm{L}} = \frac{A_{\mathrm{exp}}}{A_{\mathrm{i}}} \tag{7}$$

where A_{L}, A_{exp}, and A_{i} are, respectively, the real parts of the Fourier transforms of the structural, experimental, and instrumental diffraction peak profiles. Assuming that the finite grain size and lattice distortions are the main sources of X-ray diffraction peak broadening, A_{L} is given by classical Warren–Averbach equation [15]:

$$\ln A_{\mathrm{L}} = \ln A_{\mathrm{L}}^{\mathrm{S}} - 2\pi^2 L^2 K^2 \left\langle \varepsilon_K^2 \right\rangle \tag{8}$$

where $A_{\mathrm{L}}^{\mathrm{S}}$ is the Fourier size coefficient, $\left\langle \varepsilon_K^2 \right\rangle$ is the mean square strain, and L is the Fourier length which is defined as $L = na_3$, in which, $n = 0, 1, 2, \ldots$ and a_3 is the unit of length in the direction of K as given by:

$$a_3 = \frac{\lambda}{2(\sin\theta_2 - \sin\theta_1)} \tag{9}$$

where $\theta_2 - \theta_1$ is the angular width of the measured diffraction profile. There are various sources of lattice strain in metallic materials, e.g. dislocations, vacancies, residual elastic stresses, stacking faults, twins, grain boundaries, etc. Assuming that dislocations are the main source of lattice strain in deformed metals, Wilkens [19, 20] attributed $\left\langle \varepsilon_K^2 \right\rangle$ to dislocation parameters by:

$$\left\langle \varepsilon_K^2 \right\rangle \cong \frac{1}{4\pi}\rho b^2 \overline{C} f(\eta) \tag{10}$$

$f(\eta)$ is the Wilkens function which, at small values of L, is given by:

$$f(\eta) = \ln\left(\frac{R_{\mathrm{e}}}{L}\right) \tag{11}$$

wherein R_{e} is the effective outer cut-off radius of dislocations. By inserting Eq. 10 into Eq. 8, the modified Warren–Averbach equation is obtained [17]:

$$\ln A_{\mathrm{L}} = \ln A_{\mathrm{L}}^{\mathrm{S}} - \rho\frac{\pi b^2}{2} L^2 \ln\left(\frac{R_{\mathrm{e}}}{L}\right)\left(K^2\overline{C}\right) + O(K^2\overline{C})^2 \tag{12}$$

where O stands for higher order of $K^2\overline{C}$. Accordingly, Fourier size coefficient at different values of L is determined by extrapolating the modified Warren–Averbach plot at $K^2\overline{C} = 0$. The intercept of the initial slope at $A_{\mathrm{L}}^{\mathrm{S}} = 0$ gives the area-weighted mean column length L_0. Furthermore, by defining $M(L)$ as:

$$M(L) = \rho\frac{\pi b^2}{2} L^2 \ln\left(\frac{R_{\mathrm{e}}}{L}\right) \tag{13}$$

and, then, dividing Eq. 13 by L^2, a linear relationship between $\frac{M(L)}{L^2}$ vs. $\ln(L)$ is obtained as:

$$\frac{M(L)}{L^2} = \rho\frac{\pi b^2}{2}\left[\ln(R_{\mathrm{e}}) - \ln(L)\right] \tag{14}$$

Consequently ρ and R_{e} can be obtained by plotting the left-hand side of Eq. 14 vs. $\ln(L)$. Furthermore, a mean dislocation spacing of $\rho^{-\frac{1}{2}}$ and a dislocation arrangement parameter of $M = R_{\mathrm{e}}\sqrt{\rho}$ are determined where M values less and larger than unity indicate strong and weak dipole character of dislocations, respectively.

Results

A bright-field transmission electron micrograph of the equal-channel angular pressed 18Ni maraging steel is shown in Fig. 1, exhibiting a severely deformed structure consisting of equiaxed and elongated dislocation cell blocks with a high density of dislocations. Inset shows corresponding selected-area electron diffraction pattern, representing a relatively random orientation of dislocation cells. An X-ray diffraction spectrum obtained from the equal-channel angular pressed steel is shown in Fig. 2a which indicates body-centered cubic (bcc) iron diffraction lines. Normalized diffraction data points are shown in Fig. 2b, with superimposed Gaussian–Cauchy curves fitting to the experimental intensities. Differences between the measured data points and the fitted functions are plotted in the lower part of the figure with the same scaling as in

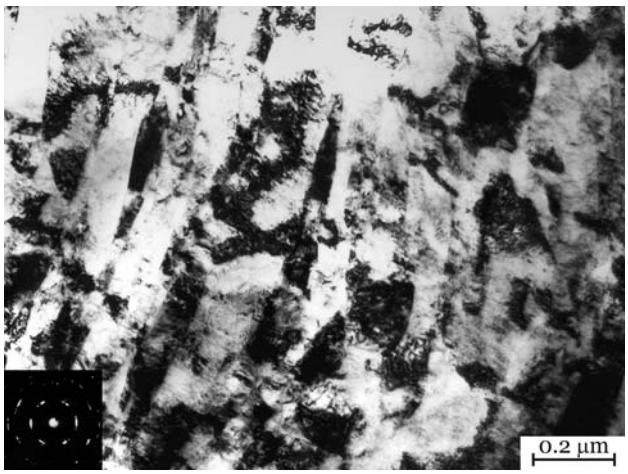

Fig. 1 Bright-field transmission electron micrograph of the equal-channel angular pressed 18Ni maraging steel. Inset shows corresponding selected-area electron diffraction pattern

the main part of the figure. Table 1 gives the experimental, instrumental, and refined structural values of β and FWHM, extracted from the functions fitted into the experimental diffraction data. Figure 3 illustrates the classical Williamson–Hall plot of FWHM versus K, in which anisotropic broadening of (200) reflection in comparison to the neighboring (211) and (220) reflections is identified. Assuming elastic constants of $C_{11} = 185.3$ GPa, $C_{12} = 109.1$ GPa, and $C_{44} = 114.8$ GPa [21], edge dislocations of <111> {110} and <111> {211} slip systems and screw dislocations of <111> {110} slip system, the average contrast factor of dislocations were calculated. Table 2 gives the $\overline{C}_{edge}$, $\overline{C}_{screw}$, and $\overline{C}_{avg}$ in which the average values were obtained assuming an equal proportion of edge and screw type dislocations. Consequently, theoretical values of q for pure edge and pure screw dislocations of the present steel were determined as 1.25 and

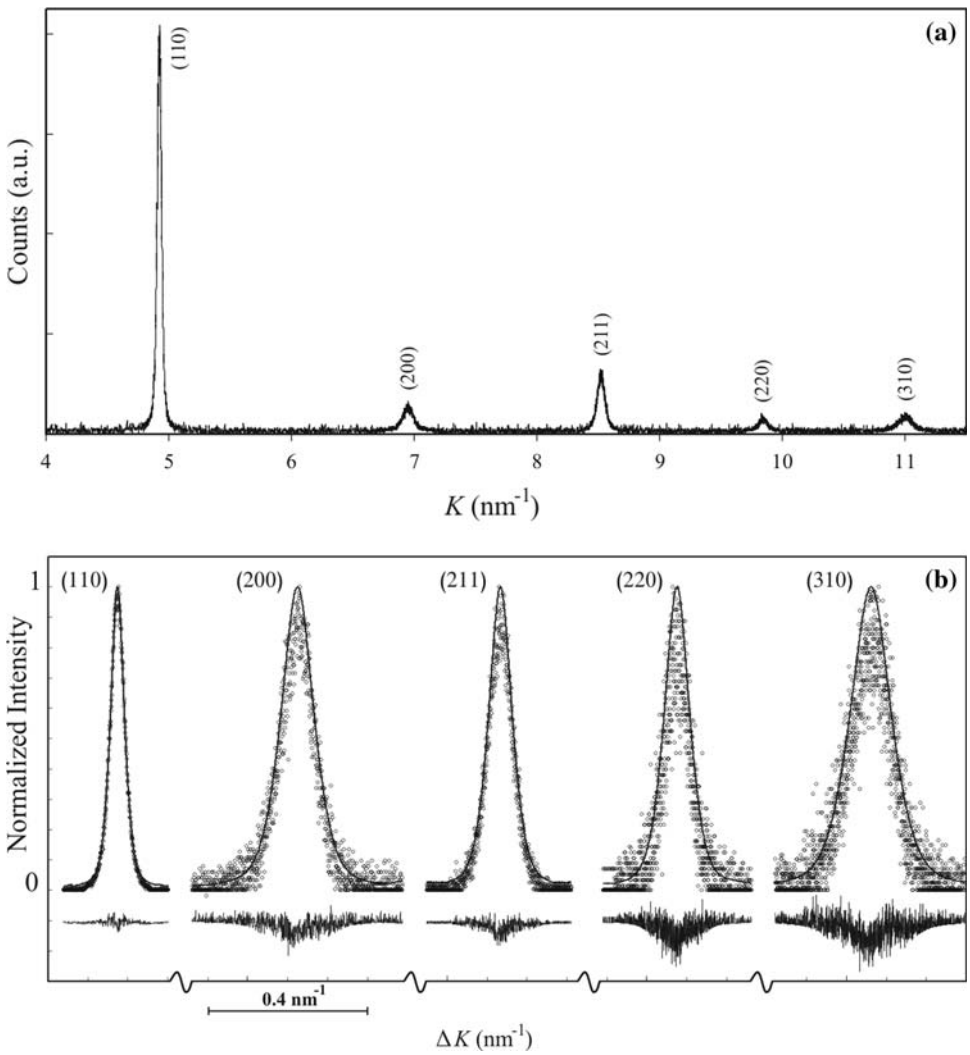

Fig. 2 **a** X-ray diffraction spectrum of the equal-channel angular pressed steel; **b** normalized experimental intensities with superimposed Gaussian—Cauchy curves fitting to the experimental intensities. In the lower part of the figure, differences between the measured data points and fitted functions are shown

Table 1 The instrumental, experimental, and structural values of diffraction peak breadths[a]

Diffraction line	Gaussian function		Cauchy function		Structural[b]
	Instrumental β (FWHM)	Experimental β (FWHM)	Instrumental β (FWHM)	Experimental β (FWHM)	β (FWHM)
(110)	0.0477 (0.0449)	0.0239 (0.0225)	0.0561 (0.0357)	0.0235 (0.0150)	0.0370 (0.0297)
(200)	0.1138 (0.1069)	0.0439 (0.0412)	0.1341 (0.0854)	0.0506 (0.0322)	0.0942 (0.0759)
(211)	0.0811 (0.0762)	0.0219 (0.0206)	0.0955 (0.0608)	0.0333 (0.0212)	0.0701 (0.0565)
(220)	0.0872 (0.0819)	0.0237 (0.0223)	0.1046 (0.0666)	0.0336 (0.0214)	0.0775 (0.0620)
(310)	0.1409 (0.1324)	0.0379 (0.0356)	0.1681 (0.1070)	0.0594 (0.0378)	0.1222 (0.0984)

[a] All peak breadths are given in nm^{-1}

[b] Average of refined Gaussian and Cauchy breadths

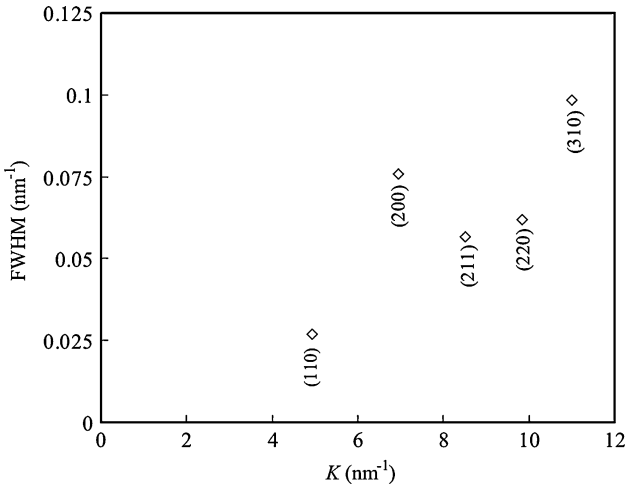

Fig. 3 A plot of FWHM vs. K, representing anisotropic broadening of (200) diffraction line

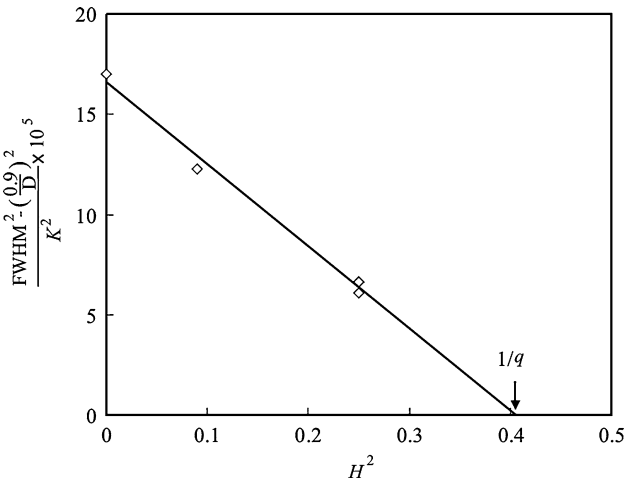

Fig. 4 Plotted according to Eq. 6, showing the dislocation parameter q obtained for the steel studied

Table 2 Values of $\overline{C}_{edge}$, $\overline{C}_{screw}$, and $\overline{C}_{avg}$ obtained for diffraction lines of the steel studied

Diffraction line	$\overline{C}_{edge}$	$\overline{C}_{screw}$	$\overline{C}_{avg}$
(110)	0.17998	0.1053	0.14265
(200)	0.26212	0.3255	0.29382
(211)	0.17998	0.1053	0.14265
(220)	0.17998	0.1053	0.14265
(310)	0.23254	0.2462	0.23938

2.71, respectively. A linear regression between the left-hand side of Eq. 6 and H^2 is shown in Fig. 4, denoting an experimental value of $q = 2.47$, as illustrated in the plot. In comparison to the theoretical values of q, the fractions of screw and edge dislocations are determined 83% and 17%, respectively, denoting about 5:1 ratio of screw to edge type dislocations. Figure 5 shows the modified Williamson–Hall plots in which FWHM and β are plotted vs. $K^2\overline{C}$. Extrapolating the regressions of β and FWHM at $K^2\overline{C} = 0$ gives the apparent size parameters of $d = 72$ nm and $D = 75$ nm, respectively. It is noteworthy to point out the difference between the apparent size parameters d and D which could be attributed to the different approaches used for derivation of peak breadths. The modified Warren–Averbach plot of ln A_L vs. $K^2\overline{C}$, according to Eq. 12, is shown in Fig. 6a. By extrapolation of ln A_L at $K^2\overline{C} = 0$ for $L = 5$, 15, 25, and 50 nm, the Fourier size coefficient A_L^S was determined. Figure 6b shows a plot of A_L^S vs. L. Considering the virtually decreasing slope of A_L^S at $L < 10$ nm, the data points between $L = 10$ nm and $L = 30$ nm were fitted into a line, the intercept of which with horizontal axis gives an area-weighted column length of $L_0 = 32$ nm. Accordingly, a plot of $M(L)/L^2$ vs. ln (L) was derived as shown in Fig. 7 from which, ρ and R_e were determined as 1.3×10^{16} m^{-2} and 40 nm, respectively. Following that, the average dislocation spacing and the dislocation arrangement parameter M were obtained about 8.6 and 4.63 nm, respectively.

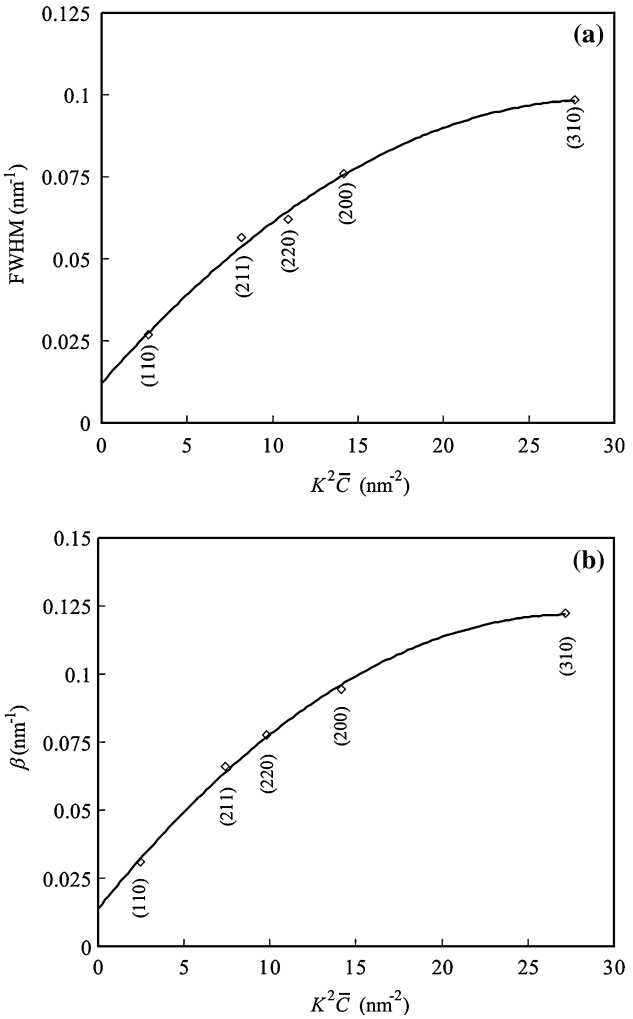

Fig. 5 Plots of **a** FWHM; **b** β vs. $K^2\overline{C}$, representing apparent size parameters

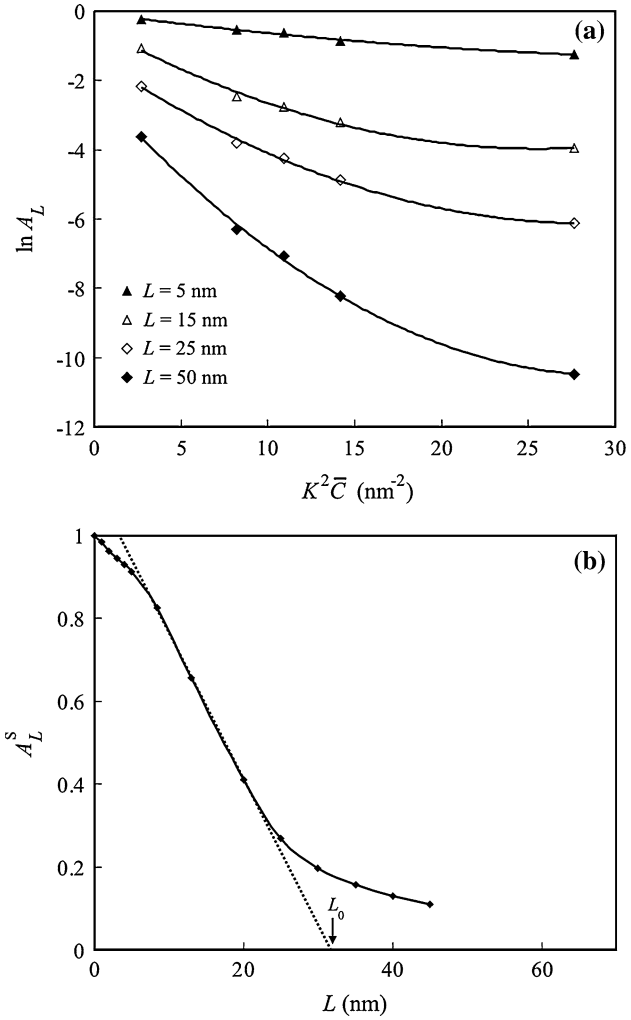

Fig. 6 Plots of **a** $\ln A_L$ vs. $K^2\overline{C}$; **b** A_L^S vs. L, giving the area-weighted column length L_0

Discussion

Transmission electron microscopy observation of the severely deformed steel represented the formation of equiaxed and elongated dislocation cell blocks. X-ray diffraction peak profile analysis of the deformed structure explored quantitative details which could be compared with the solution-annealed martensitic state [14] as given in Table 3. It is found that upon equal-channel angular pressing of lath martensite; (i) the average of the three apparent grain sizes decreases from about 156 to about 60 nm, (ii) dislocation density increases from 0.7×10^{16} m^{-2} up to 1.3×10^{16} m^{-2}, (iii) the dislocation parameter q increases from 2.01 to 2.47, representing that the volume fraction of screw dislocations increases from about 50% up to 83%, (iv) mean dislocation spacing decreases from 11.8 to 8.6 nm and correspondingly the

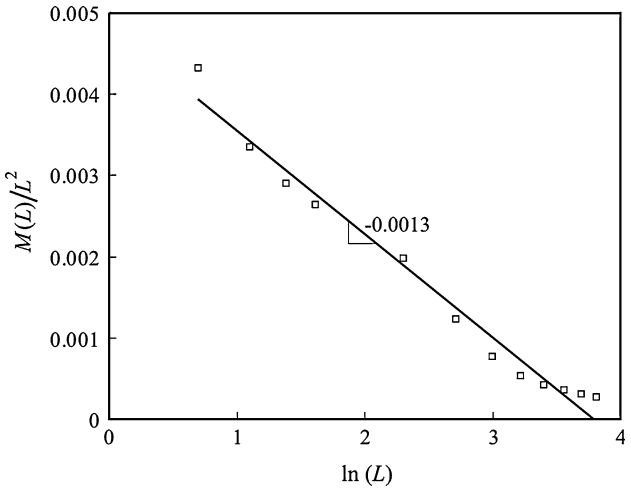

Fig. 7 Plot of $\frac{M(L)}{L^2}$ vs. ln(L), used for determination of ρ and R_e according to Eq. 14

Table 3 Microstructural parameters of the solution-annealed and deformed 18Ni steels determined by X-ray diffraction peak profile analysis

Steel	d (nm)	D (nm)	L_0 (nm)	ρ ($\times 10^{16}$ m^{-2})	$\rho^{-1/2}$ (nm)	R_e (nm)	M	q
Solution-annealed	175 ± 24	150 ± 15	143 ± 8	0.7 ± 0.03	11.8 ± 0.02	63 ± 9	5.36 ± 0.8	2.01 ± 0.02
Deformed	72 ± 5	75 ± 7	32 ± 2	1.3 ± 0.03	8.6 ± 0.01	40 ± 5	4.63 ± 0.6	2.47 ± 0.02

effective outer cut-off radius of dislocations decreases from 63 down to 40 nm, (v) the arrangement parameter of dislocations M decreases from 5.36 to 4.63, representing that the dipole character and thus the screening action of strain fields of multiple dislocations increases by equal-channel angular pressing.

It has been well recognized that the apparent size parameter determined by X-ray diffraction analysis is equivalent to the coherently scattering crystalline domains size which are separated from each other by small misorientations, at least for one or two degrees [22]. Studies on the structure of deformed metals have clarified that there are hierarchically multiscaled crystalline domains in the deformed structures; (i) submicrometer-sized dislocation cell blocks separated by geometrically necessary dislocation boundaries with relatively high angles of misorientation, (ii) nanocrystalline subgrains or dislocation cells separated by incident dislocation boundaries with low angles of misorientation, as the latter posses the highest frequency in the microstructure [23, 24]. In a deformed structure, it is reasonable to propose that the dislocation cells contribute substantially to incoherent scattering of X-ray, acting as the most predominant source of size-induced peak broadening. Therefore, the apparent grain size determined for the present steel is likely to represent the dislocation cell size. A mean dislocation cell size of about 50 nm was obtained from Fig. 1, via counting the intercept number of transverse lines crossing the lamellar boundaries. Consequently, a correlation between the X-ray diffraction results and transmission electron microscopy observation can be deduced in the present study. In accordance with the experimental results, it is understood that four passes of equal-channel angular pressing develops a deformed structure consisting of equiaxed or elongated dislocation cell blocks with a mean size of a few hundred nanometers. The dislocation cell blocks include smaller dislocation cells of less than 100 nm mean size in hierarchy. According to the aforementioned length scales, present deformed structure could be included in the ultrafine-grained or nanostructured state.

Studies on the character of prevailing dislocations in the severely deformed face-centered cubic (fcc) metals identified that the dislocation parameter q and the dislocation arrangement parameter M decrease with increasing strain [25, 26]. Consequently, it has been suggested that the fraction of edge dislocations increases at large strain and furthermore, the dislocation configuration turns to low-energy dislocation structures, i.e. significant reduction occurs in the total strain energy associated with dislocations at large strain. It has also been identified that the fraction of 1/6 <112> {111}-type partial dislocations increases in a commercial-purity copper deformed by cold-rolling up to 90% thickness reduction at liquid nitrogen [27]. However, it is found that the dislocation parameter q and hence, the relative fraction of screw dislocations increase by increased straining of the present bcc metal, in contrast to the fcc metals. The controversy may be attributed to the differences in slip systems in association with intrinsic high stacking faults energy of the present steel, favoring the cross-slipping of dislocations to be accomplished by activation and generation of screw dislocations. The high values of dislocation arrangement parameter M obtained for the solution-annealed and the deformed 18Ni (300) maraging steels represent that the dislocations have weak dipole character, suggesting a relatively rigid dislocation configurations of weakly-screening strain fields. However, decreasing of M value in the deformed steel indicates that the dislocation arrangement goes toward the formation of low-energy dislocation structures, acting as an initial step in the formation of dislocation cells and ultrafine grains. Accordingly, it is found that further straining of the present steel is necessary for the development of randomly oriented ultrafine grains.

Conclusions

Effect of equal-channel angular pressing on the microstructure of an 18Ni maraging steel was studied by means of X-ray diffraction peak profile analysis. The main conclusions are:

1. A mean grain size of about 60 nm was determined, corresponding reasonably to the dislocation cell size observed by means of transmission electron microscopy.
2. A dislocation density of 1.3×10^{16} m^{-2} along with about 5:1 ratio of screw to edge type dislocations were identified.
3. The dislocation arrangement parameter represented weak dipole and thus weak screening action of the strain fields of dislocations.

4. In comparison to the starting lath martensite, apparent grain size decreases, dislocation density and fraction of screw dislocations increase, and the dipole character of dislocations decreases leading to a decrease in total strain energy associated with dislocations.

References

1. Valiev RZ, Islamgaliev RK, Alexandrov IV (2000) Prog Mater Sci 45:103. doi:10.1016/S0079-6425(99)00007-9
2. Langdon TG (2007) Mater Sci Eng A 462:3. doi:10.1016/j.msea.2006.02.473
3. Zhu YT, Langdon TG (2005) Mater Sci Eng A 409:234. doi:10.1016/j.msea.2005.05.111
4. Tsuji N, Ueji R, Minamino Y, Saito Y (2002) Scr Mater 46:305. doi:10.1016/S1359-6462(01)01243-X
5. Das SK, Thomas G (1970) Metall Trans 1:325. doi:10.1007/BF02642804
6. Morito S, Huang X, Maki T, Hansen N (2006) Acta Mater 54:5323. doi:10.1016/j.actamat.2006.07.009
7. Morito S, Nishikawa J, Maki T (2003) ISIJ Int 43:1475. doi:10.2355/isijinternational.43.1475
8. Morito S, Iwamoto S, Maki T (2003) In: Takeuchi H (ed) Int. Forum for the properties and applications of IF steels. The Iron Steel Institute of Japan, Tokyo
9. Ueji R, Tsuji N, Minamino Y, Koizumi Y (2002) Acta Mater 50:4177. doi:10.1016/S1359-6454(02)00260-4
10. Tianfu J, Yuwei G, Guiying Q, Quan L, Tiansheng W, Wei W et al (2006) Mater Sci Eng A 432:216. doi:10.1016/j.msea.2006.06.047
11. Hossein Nedjad S, Nili Ahmadabadi M, Furuhara T (2008) Mater Sci Eng A 485:544. doi:10.1016/j.msea.2007.08.008
12. Iranpour Mobarake M, Nili Ahmadabadi M, Poorganji B, Fatehi A, Shirazi H, Furuhara T, Habibi Parsa M, Hossein Nedjad S (2008) Mater Sci Eng A 491:172. doi:10.1016/j.msea.2008.02.034
13. Ungar T, Gubicza J, Hanak P, Alexandrov IV (2001) Mater Sci Eng A 319–321:274. doi:10.1016/S0921-5093(01)01025-5
14. Hossein Nedjad S, Movaghar Gharabagh MR (2007) Int J Mater Res (accepted)
15. Warren BE (1969) X-ray diffraction. Addison Wesley, Massachusetts
16. Ribarik G, Ungar T, Gubicza J (2001) J Appl Cryst 34:669. doi:10.1107/S0021889801011451
17. Ungar T, Gubicza J, Ribarik G, Borbely A (2001) J Appl Cryst 34:298. doi:10.1107/S0021889801003715
18. Ungar T, Dragomir IC, Revesz A, Borbely A (1999) J Appl Cryst 32:992. doi:10.1107/S0021889899009334
19. Wilkens M (1967) Acta Metall 15:1412. doi:10.1016/0001-6160(67)90020-X
20. Wilkens M (1969) Acta Metall 17:1155. doi:10.1016/0001-6160(69)90092-3
21. Chaudari DK, Ravindran PA, Wert JJ (1972) J Appl Phys 43:778. doi:10.1063/1.1661280
22. Ungar T, Ribarik G, Gubicza J, Hanak P (2002) Trans ASME 124:2
23. Kuhlmann-Wilsdorf D, Hansen N (1991) Scr Metall Mater 25:1557. doi:10.1016/0956-716X(91)90451-6
24. Li BL, Godfrey A, Meng QC, Liu Q, Hansen N (2004) Acta Mater 52:1069. doi:10.1016/j.actamat.2003.10.040
25. Fatay D, Bastarash E, Nyilas K, Dobatkin S, Gubicza J, Ungar T (2003) Z Metallkd 94:1
26. Gubicza J, Balogh L, Hellmig RJ, Estrin Y, Ungar T (2005) Mater Sci Eng A 400–401:334. doi:10.1016/j.msea.2005.03.042
27. Dragomir IC, Gheorghe M, Thadhani N, Snyder RL (2005) Mater Sci Eng A 402:158. doi:10.1016/j.msea.2005.04.028